Available online at www.sciencedirect.com

ScienceDirect

Procedia Structural Integrity 57 (2024) 754–761

Structural Integrity Procedia

www.elsevier.com/locate/procedia

Fatigue Design 2023 (FatDes 2023)

Fatigue life assessment of a slender lightning rod due to wind excited vibrations

Andi Xhelaj [a]*), Andrea Orlando [a]), Luisa Pagnini [a]), Federica Tubino [a]), Maria Pia Repetto [a])

[a]) *Department of Civil, Chemical and Environmental Engineering, University of Genoa, Italy*

Abstract

The wind-excited vibrations of structures induce fluctuating stresses that may result in the accumulation of fatigue damage, ultimately posing a risk of structural failure. This paper presents the findings of a research program assessing the fatigue life of a 30 m high slender and tapered lightning pole under wind induced vibrations. A three-stage study has been conducted to understand the causes of fatigue damage. In the first step, a hybrid numerical and full-scale experimental investigation was carried out to identify the natural frequencies, modal shapes and modal damping ratios. In the second step, results from the dynamic identification test were used to estimate vortex shedding induced vibrations. Critical resonant conditions on the first and second vibration modes have been investigated, adopting standards and calculation techniques from literature. Finally, in the third step, the fatigue damage induced by vortex shedding vibrations was estimated. The findings demonstrate that the fatigue issues of the lightning rod are mainly related to the wind induced stress at the base of the pole, highlighting the contribution of vortex shedding resonant with the second vibration mode. The paper also discusses the large uncertainties affecting the analysis, showing that errors in parameter estimates give rise to very large scatter in the fatigue damage assessment.

Keywords: Fatigue Damage; Vortex Induced Vibrations (VIV); Lightning Rod; Parameter Uncertainity in Fatigue Assessment.

1. Introduction

Wind-excited vibrations of structures can induce damage accumulation and cause structural failure without exceeding ultimate limit states (Repetto and Solari, 2002). Several cases of damage and collapse have been observed for different kind of structures such as guyed masts, cantilever steel structures and especially poles (Repetto and Solari, 2010). Slender vertical structures exposed to wind may experience vortex-induced crosswind vibrations which are often more

* Corresponding author. Tel.: +39 010 3352491; fax: +39 010 3352491.
E-mail address: andi.xhelaj@edu.unige.it

10.1016/j.prostr.2024.03.081

critical than the alongwind vibrations (Pagnini and Piccardo, 2017), representing one of the main sources of the damage accumulation due to fatigue for a wide variety of slender vertical structures (e.g., Orlando et al., 2021).
The current work analyzes the fatigue life performance of an existing single column lightning rod, that is part of a collective array of similar structures within an industrial site. Over a decade following their installation, these lightning rods have experienced significant structural issues. One of them suffered a complete collapse, while several others exhibited unexpected cracks at the connection between the pole and the base plate. Cracks were identified through non-destructive diagnostic investigations and were attributed to underlying fatigue damage, which raised high concerns regarding the long-term structural integrity of the lightning rod array. Consequently, a research activity started with the objective of comprehensively studying the fatigue induced on these structures by the dynamic action of wind, as well as exploring effective measures for mitigating vibrations. This research paper presents the key findings resulting from the endorsed research activity.
This paper is organized as follows: after these brief introductory notes, Section 2 provides a comprehensive description of the geometrical and dynamic properties of the examined structure. Its characterization was obtained through numerical analysis and an on-site dynamic identification test campaign conducted in November 2022. Section 3 presents the findings of the analysis conducted to evaluate the dynamic response of the structure when subjected to wind-induced actions, with the ultimate purpose of estimating the fatigue life caused by vortex induced vibrations (VIV), in accordance with the most advanced regulatory guidelines and standards in the field. Section 4 provides a comprehensive analysis of the uncertainties in the VIV fatigue life assessment, focusing on structural damping estimate and the choice of fatigue curve. Lastly, Section 5 provides the main conclusions derived from this research activity, summarizing the key insights and implications drawn from the study.

2. Lightning rod characterization

2.1. Geometrical and mechanical characteristics

The structure analyzed is a S355 steel pole with a tapered regular 16-sided polygonal section (Fig. 1). It has a total height of 30 m. The shaft is composed of three trunks superimposed by slip joints (Fig. 1b); the thickness is constant along the entire height, and it is equal to 0.004 m. The outer diameter of the cross-section varies from 0.77 m at the base to 0.24 m at top. The base constraint is realized through a flanged joint: a plate with 930 mm outer diameter and 30 mm thickness is welded to the shaft with internal and external angle bead welding and attached to the foundation nut with 22 S355 steel anchor bolts (Fig. 1c). The pole is free of any appendages or ancillaries along its height.

2.2. Dynamic characteristics

Dynamic parameters such as natural frequencies, modal shapes, and damping ratios are fundamental in evaluating dynamic response and fatigue life assessment. For the structure under investigation, they were determined using a blend of numerical simulation with a Finite Element Model (FEM), supplementary guidelines from CNR-DT 207/R1 2018 (CNR, 2019), where applicable, and experimental data, derived from full-scale pull and release tests (Fig. 2).
Given the double symmetry of the structure, paired vibrational modes occur in two orthogonal vertical planes with almost identical properties. For clarity, subsequent references to natural frequencies, modal shapes, and damping parameters pertain to a single plane, but can be considered representative for the orthogonal counterpart as well. Table 1 provides the natural frequencies and damping ratios of the first two vibration modes. The natural frequencies were determined using both FEM calculations and experimental tests (Fig. 2 (b)). The structural damping represents one of the most important and uncertain parameters at the same time, and errors in its estimate can heavily propagate on the results (e.g., Pagnini, 2010), particularly evident in the case of fatigue analysis (Pagnini and Repetto, 2012). Therefore, in addition to the measured values, also the empirical estimates provided by the CNR-DT 207/R1 recommendations (CNR, 2019) are included in Table 1.

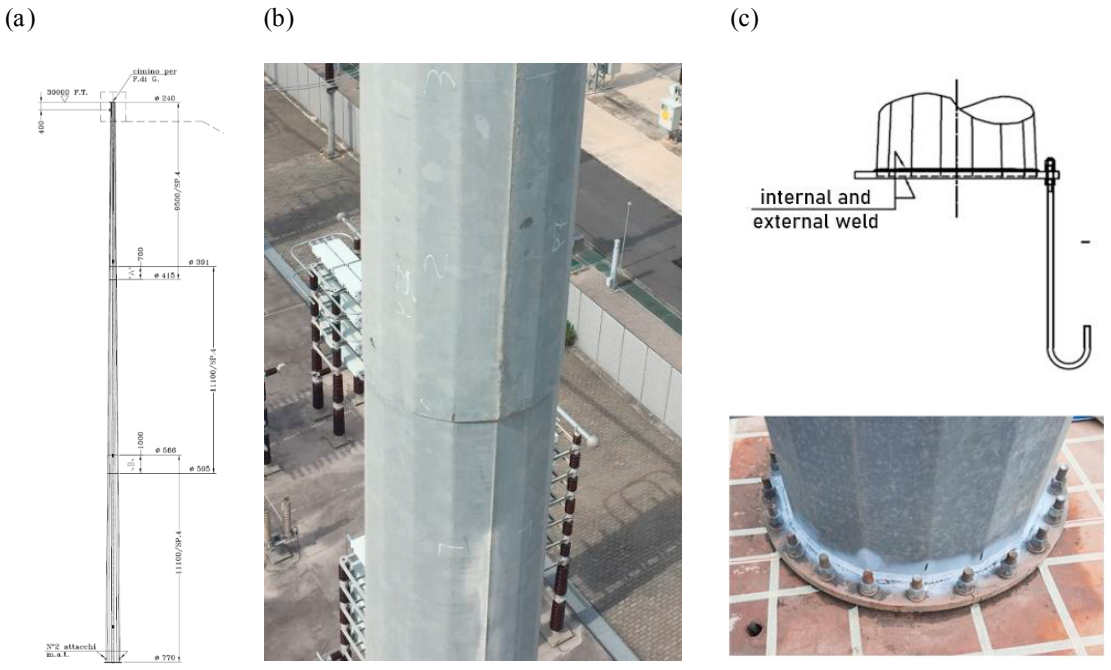

Fig. 1. Lightning rod: (a) Pole geometry; (b) Intersecting joint sections; (c) Connection between the pole and the base plate.

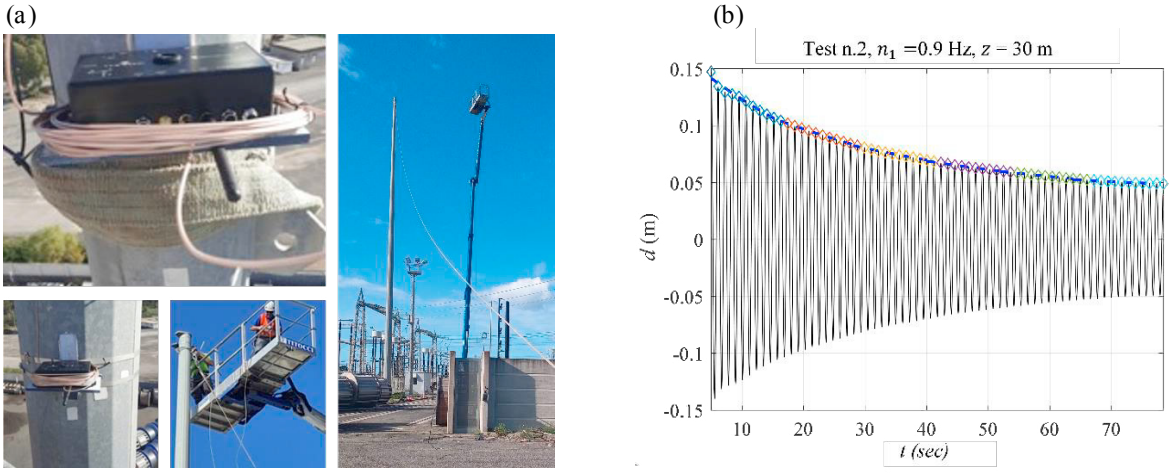

Fig. 2. Pull and release tests: (a) Picture of the tests conducted for the dynamic characterization of the lightning rod; (b) Top displacement corresponding to the first mode of vibration.

Table 1. Natural frequencies (n_j) and structural damping ($\xi_{s,i}$) of the lightning rod.

Mode i	n_i [Hz] (FEM)	n_i [Hz] (Experimental)	$\xi_{s,i}$ [%] (Experimental)	$\xi_{s,i}$ [%] (CNR, 2019)
1	1.00	0.90	0.30	0.20
2	4.13	3.60	0.10	0.20

Table 1 reveals that measured natural frequencies are approximately 10% lower than the FEM estimates. This deviation is attributed to the flexibility of the base constraint, which differs from the fixed constrain used in the numerical model. Hence, the evaluation of fatigue life is carried out using the values of fundamental frequencies obtained from the experimental campaign. The experimental modal damping for the first vibration mode aligns with or slightly surpasses the recommended value from the reference standard (CNR, 2019). For the second vibration mode, it falls below the normative value, likely due to the structural simplicity, linearity, and absence of dissipative elements (Fig. 3 (a)), representing therefore a key concern for the examined structure. The modal shapes could not be reliably identified by the full-scale measurements; therefore, they were evaluated numerically through a finite element model of the structure created in MATLAB (Fig. 3).

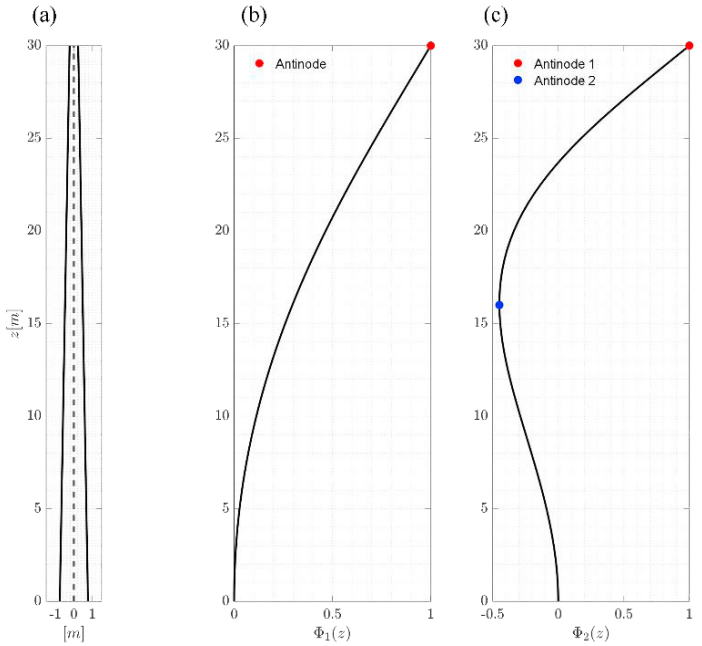

Figure 3. (a) Schematic of the tapered lightning rod. First (b) and second (c) modal shape of the lightning rod. The positions of the antinodes (minimum or maximum values within the modes) are also shown with red (top antinode) and blue (intermediate antinode) dots.

3. Dynamic response and fatigue life assessment due to vortex induced vibrations

3.1. Dynamic response due to vortex induced vibrations

Vortex-Induced Vibration is a significant phenomenon in Wind Engineering, particularly for slender and lightweight structures. The resulting oscillating pressures on the body surface generate fluctuating forces perpendicular to the mean flow direction that can be particularly influential for slender structures. Engineering verifications (e.g., EN 1991-1-4, 2005, CNR, 2019) commonly use two calculation procedures. The spectral model (Vickery and Basu, 1983) supplies an analytical expression for an equivalent aerodynamic damping; however, for VIV resonant with higher vibration modes, it does not yet find a codified procedure. The harmonic model (Ruscheweyh, 1994) supplies a vortex-induced force. It is calibrated on experimental data from a broad range of structures, but can overestimate vortex shedding effects at very low Scruton numbers (Hansen, 1999). For this reason, in the current work, VIV is investigated using the harmonic model, following the procedure outlined in the CNR-DT 207/R1 guidelines (CNR, 2019).
The critical wind velocity of vortex shedding in the *i*-th cross-wind mode is given by:

$$v_{\mathrm{cr},i} = \frac{n_i \cdot b}{St} \tag{1}$$

where n_i is the i-th natural frequency associated with the i-th vibration mode perpendicular to the mean wind direction; St is the Strohual number and b is the reference size of the cross-section where critical vortex shedding occurs. The peak deflection $y_{p,i}$ induced by the critical vortex shedding in the i-th across-wind vibration mode is given by:

$$y_{p,i} = \frac{1}{S_t^2} \cdot \frac{1}{S_{C_i}} \cdot K \cdot K_w \cdot c_{lat} \cdot b \tag{2}$$

where S_{Ci} is the Scruton number for the across-wind vibration mode i; K and K_w are, respectively, the mode shape factor and the correlation length factor; c_{lat} is the lateral wake force coefficient. The parameter that governs the VIV response is the Scruton number S_{Ci} defined as follows:

$$S_{C_i} = \frac{4\pi \cdot m_i \cdot \xi_{s,i}}{\rho \cdot b^2} \tag{3}$$

where m_i and $\xi_{s,i}$ are, respectively, the equivalent mass per unit length and the structural damping ratio in the i-th mode (Table 1), ρ is the density of air. From Equations (2) and (3), it can be deduced that the smaller is the Scruton number (and therefore the lighter and/or low damped structure), the greater is the structural response. For structures with circular sections, based on experiences from real cases, if the Scruton number is small, *e.g.*, less than 5, vibrations induced by resonant vortex shedding may arise in lock-in conditions (Pagnini et al., 2020) and be significantly dangerous. The effect of cross-wind VIV in the i-th mode can be calculated through the application of the equivalent static force per unit length, orthogonal to the average wind direction and to the axis of the structure. It is given by:

$$F_i(z) = \mu(z) \cdot (2\pi \cdot n_i)^2 \Phi_i(z) \cdot y_{p,\mathrm{i}} \tag{4}$$

where z is the coordinate along the structure axis, μ is the mass per unit length of the structure, n_i is the i-th natural frequency of the structure, Φ_i is the i-th modal shape. The application of the equivalent static force allows the evaluation of the corresponding bending moment $M_{b,i}$ and the nominal stress at the base of the pole $\sigma_{b,i}$. For the second across-wind vibration mode, two different load conditions should be considered, assuming resonant vortex shedding at the level of antinode 1 and antinode 2 (Fig. 3). In the calculations, damping ratio for the first mode is assumed according to the CNR 2019 guidelines, i.e., $\xi_{s,1}$ = 0.2%; for the second mode, $\xi_{s,2}$ = 0. 1%, derived from the experimental campaign. Table 2 provides an overview of the obtained values.

Table 2. Calculation of the dynamic response due to vortex shedding resonant on the first and second across -wind vibration mode.

Mode i	n_i [Hz]	b [m]	St [-]	$v_{cr,i}$ [m/s]	$\xi_{s,i}$ [%]	S_{Ci} [-]	K [-]	K_w [-]	c_{lat} [-]	$y_{p,i}$ [m]	$M_{b,i}$ [kNm]	$\sigma_{b,i}$ [N/mm^2]
1	0.9	0.24	0.19	1.14	0.20	11.15	0.129	0.134	0.7	0.007	1.80	0.98
2 -Antinode 1	3.6	0.24	0.19	4.55	0.10	6.53	0.177	0.307	0.7	0.038	34.60	18.85
2 -Antinode 2	3.6	0.49	0.19	9.28	0.10	1.57	0.177	0.292	0.7	0.580	504.53	275.00

Due to the lightweight nature of the structure and the notably low value of structural damping, Table 2 shows very low Scruton numbers, highlighting possible criticalities especially concerning VIV resonant with mode 2 at the level of antinode 2 (Fig. 3).

3.2. Fatigue life assessment due to VIV.

Fatigue assessment is carried out adopting the classical S-N approach, with reference to the base welded joint (see Fig. 1 (c)). Referring to Eurocode 3– Part 1-9: Fatigue (EN 1993-1-9, 2005), the detail under examination is associated with category 40 as fatigue class. Therefore, the fatigue resistance curve, represented as a trilinear curve in a bi-

logarithmic diagram, is characterized by a nominal stress amplitude equal to $\Delta\sigma_c$ = 40 N/mm^2 at N_c=2 10^6 cycles to failure. From this curve it is also possible to determine the cut-off limit, i.e., the amplitude of cycles below which the stress does not induce fatigue damage, given by $\Delta\sigma_D$= 29.5 N/mm^2 for cycles with constant amplitude, $\Delta\sigma_L$= 16.2 N/mm^2 for cycles with variable amplitude. The structural response to each critical speed is assumed to be sinusoidal (i.e., the applied stress cycles have constant amplitude). The number of load cycles, N_i, induced by resonant VIV in the i-th mode of vibration, is given by (EN 1991-1-4, 2005, CNR, 2019):

$$N_i = 2 \cdot V_N \cdot \mathrm{n}_i \cdot \varepsilon_0 \cdot \left(\frac{v_{cr,\mathrm{i}}}{v_{0,i}}\right)^2 \cdot \exp\left[-\left(\frac{v_{cr,\mathrm{i}}}{v_{0,i}}\right)^2\right] \tag{5}$$

where V_N (= 50 years) is the nominal life of the structure, ε_0(=0.3) is the bandwidth amplitude factor, $v_{cr,i}$ is the i-th critical speed of vortex-shedding, $v_{0,i}$ is a reference value for the wind speed and is provided by the CNR 2019 guidelines. Assuming V_N equal to 1 year, Equation (5) gives the number of cycles/years accumulated by the structure. The annual fatigue damage is given by:

$$D(1) = \frac{N_i(V_N = 1year)}{N_r} \tag{6}$$

where N_r is the number of cycles to failure for the nominal stress induced by vortex-shedding, obtained from fatigue resistance curves of the structural detail in correspondence of the VIV induced nominal stress amplitude $\Delta\sigma_{bi} = 2 \cdot \sigma_{bi}$. The fatigue lifetime T_F is obtained by inverting Equation (6), T_F = *1/D(1)*. Table 3 summarizes the results of fatigue life assessment for vortex shedding resonant with the first two vibration modes.

Table 3. Fatigue life assessment for a detail category $\Delta\sigma_c$ = 40 N/mm^2 due to vortex shedding resonant with the first two modes of vibration.

Mode i	$\Delta\sigma_{b.Li}$ [N/mm^2]	N_i [cycles/year]	N_r [cycles/failure]	T_F [years]
1	1.96	$5.05 \cdot 10^5$	∞	∞
2 – Antinode 1	37.70	$2.05 \cdot 10^7$	$2.383 \cdot 10^6$	<1
2 – Antinode 2	550.00	$1.89 \cdot 10^7$	- *	- *

* The calculation cannot be done since the stress amplitude is too large.

The first mode resonant VIV induced stress amplitude is lower that the cut-off limit, thus not generating fatigue damage. The second mode resonance at antinode 1 (at the top of the pole) induces small VIV stress amplitude but a very large number of cycles, thus generating high damage and a very low expected fatigue life. The second mode resonance at antinode 2 (at the intermediate level of the pole) induces very high VIV stress amplitude out of the range of the classical S-N approach, generating an almost evanishing fatigue life. Adopting the current standard methods, the structure is therefore not verified with respect to the fatigue limit state induced by the action of VIV resonant with the second mode.

4. Analysis of uncertainties in vortex shedding-induced fatigue

The uncertainty analysis is approached from a parametric perspective investigating the relationship between variations in fundamental dynamic and mechanical parameters of the structure and the resulting changes in fatigue damage or the fatigue life of the lightning rod. Accordingly, this analysis considers the structural damping ratio $\xi_{s,i}$ as a key quantity, which is varied parametrically from 0.085% up to 1%. Additionally, three fatigue curves are employed referring to Eurocode 3– Part 1-9: Fatigue (EN 1993-1-9, 2005) to describe the behavior of the welded connection between the base plates and the rod. These fatigue curves are characterized by a nominal stress amplitude equal to $\Delta\sigma_c$ = 36 , 40 and 71 N/mm^2 at N_c=2 10^6 cycles to failure, respectively. Fig. 4 reports main results. Figure 4 (a) shows the peak stress amplitude $\Delta\sigma_{p,2}$ due to resonant vortex shedding in the second vibration mode for antinode 1 (Fig. 3(c)), calculated at the base of the pole. The figure demonstrates that as the structural damping increases (damping

ranges from 0.085% to 0.2% to improve the representation), $\Delta\sigma_{p,2}$ decreases in inverse proportion, aligning with Equations (2) and (3). In the same figure, horizontal lines represent the cut-off limits for the three different detail categories which are respectively $\Delta\sigma_D$ = 26.5 (FAT36), 29.5 (FAT40) and 52.3 (FAT71) N/mm^2. On the other hand, Fig. 4 (c) depicts the relationship between fatigue damage (expressed in logarithmic scale in the y-axis) and damping ratio; the different curves represent the considered detail categories. Damage in detail categories FAT36 and FAT40 is notably affected by the structural damping. From Fig. 4 (c), it is evident that there exists a critical damping value below which fatigue damage $D(1)$ exceeds 1, indicating a fatigue life T_F smaller than 1 year. For the resonant response at the level of the first antinode, the critical damping values result 0.138% for detail category 36 and 0.124% for detail category FAT40. Beyond these critical values, a slight increase in damping ($\Delta\xi_{s,i}$ = 0.001%) induces a sharp discontinuous transition in fatigue damage, reducing it to negligible levels and resulting in an infinite fatigue life. Furthermore, Fig. 4(c) demonstrates that for detail category FAT71 the fatigue damage is negligible, indicating an unlimited fatigue life within the specified damping range. Figure 4 (b) shows the peak stress amplitude for resonant vortex shedding in the second mode of vibration for antinode 2 (Fig. 3(c)) evaluated at the base of the pole. This is the most critical mode for the structure under examination, as can be seen from the response in terms of peak stress amplitudes, which are clearly excessive for structural damping smaller than 0.60 %. Figure 4 (d) depicts the relationship between fatigue damage and damping ratio for the three detail categories. The observed trend remains consistent, indicating three distinct critical values of structural damping for each curve, where fatigue damage changes from being significantly greater than 1 to virtually zero. These critical damping values are 0.916% for detail category FAT36, 0.862% for detail category FAT40, and 0.613% for detail category FAT71. Beyond these critical values, fatigue damage abruptly decreases to zero. From this analysis, some preliminary considerations can be made. First, notwithstanding its apparent simplicity, the structure is not verified to fatigue, for any category of detail, unless structural damping is higher than 0.60%. Structural damping of steel poles is, however, commonly below this value (e.g., Pagnini and Solari, 2001, Pagnini and Piccardo, 2021). Second, for the considered structure, the fatigue phenomenon is reduced to an activation problem. If damping is below a certain threshold, fatigue is activated and the cycles are so many that fatigue life evanishes. If damping is beyond this limit, stress amplitudes are below the cut-off limit and fatigue does not occur. Therefore, given the large uncertainties in damping evaluation, the fatigue assessment becomes quite volatile. Such results raise serious concerns about the capability of the current standards to catch the VIV fatigue phenomenon and the reliability of the final assessment, at least at quantitative level.

5. Conclusions

In this paper a study is conducted to understand the causes of fatigue damage in a group of lightning rods located within an industrial site. The analysis includes a full-scale experimental investigation of the modal parameters, calculation of the VIV-induced response, and estimation of the corresponding fatigue life. Due to its lightweight nature and notably low value of structural damping, the structure is characterized by very low Scruton numbers for the relevant vibration modes, highlighting possible criticalities concerning structural response to vortex-shedding. The calculation of fatigue life has shown that, by adopting the current standard methods, the structure is not verified with respect to the fatigue limit state induced by the action of VIV resonant with the second mode of vibration. In particular, the resonance at antinode 2, at the intermediate level of the pole, induces very high VIV stress amplitude (out of the range of the classical S-N approach), generating an almost evanishing fatigue life, much less than one year. This is clearly overconservative, since the structure under examination exhibited 10 years of service life before crack detection. The calculation has been repeated by varying structural damping and fatigue resistance of the considered detail. The results highlighted that, for the case study, the fatigue phenomenon is reduced to an activation problem: if damping is below a certain threshold, fatigue is activated and the cycles are so many that fatigue life evanishes; if damping is beyond this limit, fatigue does not occur. Considering the large uncertainties in damping estimate and in the VIV amplitude evaluation, the fatigue assessment may undergo large variations to the point that the structure can be safe or unsafe by varying the damping even slightly. In any case, beyond the unreliable quantitative value, the applied regulatory methodology is able to highlight structural criticalities, allowing the identification of the cause of the detected fatigue damage.

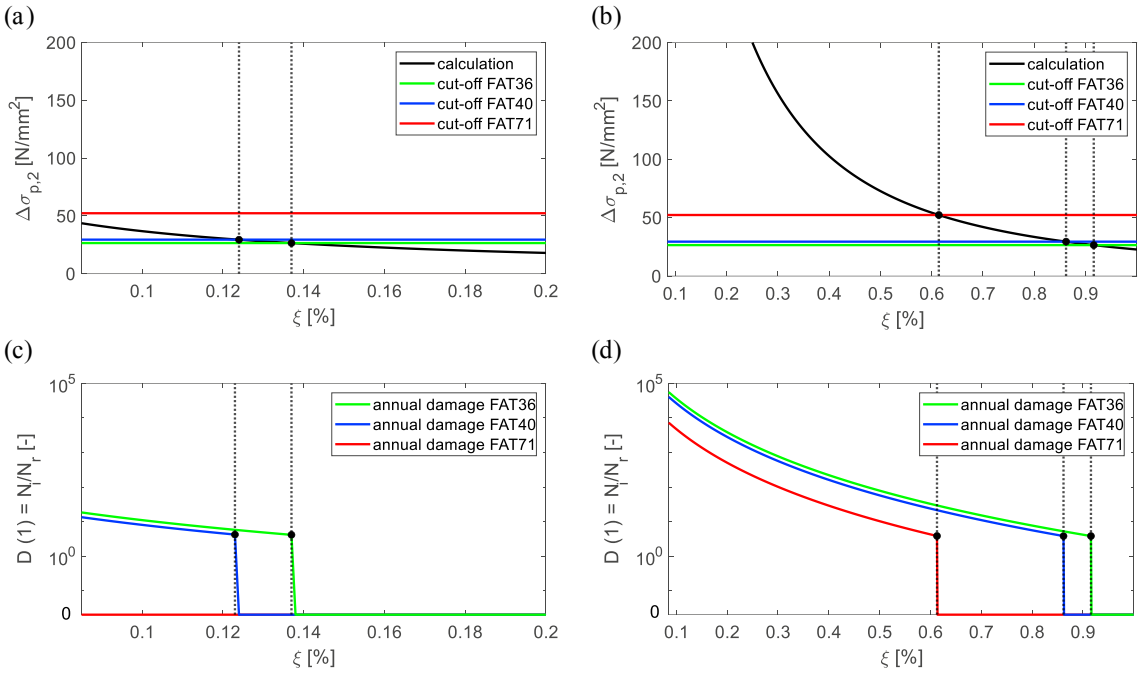

Fig. 4. Dynamic response to resonant vortex shedding as a function of the structural damping for the second vibration mode at the height of antinode 1 (a) and antinode 2 (b). Fatigue damage expressed in logarithmic scale as a function of the structural damping and three different detail categories for mode 2 evaluated at antinode 1 (c) and antinode 2 (d). The black dotted lines indicate the abrupt passages from fatigue damage greater than one to zero damage.

Acknowledgements

The Authors gratefully acknowledge CTE SPA organization and its Technical Director eng. Massimiliano Tassistro for the invaluable support and generous availability throughout the course of this research.

References

CNR, 2019. Instructions for the evaluation of the actions and effects of wind on buildings - CNR-DT 207/R1 2018. National Research Council, Rome.
EN 1991-1-4, 2005. Eurocode 1: Actions on Structures - Part 1.4: General Actions - Wind Actions. CEN, European Committee for Standardization, Brussels, Belgium.
EN 1993-1-9 (2005). Eurocode 3: Design of Steel Structures -Part 1-9: Fatigue, CEN, European Committee for Standardization, Brussels, Belgium.
Hansen, S.O., 1999. Vortex induced vibrations of line-like structures. CICIND Rep. 15 (1), 15–23.
Orlando, A., Pagnini, L, Repetto, M.P., 2021. Structural response and fatigue assessment of a small vertical axis wind turbine under stationary and non-stationary excitation. Renewable Energy 170, 251-266.
Pagnini, L., 2010. Reliability analysis of wind excited structures. Journal of Wind Engineering and Industrial Aerodynamics 98 (1), 1-9.
Pagnini, L., Repetto, M.P., 2012. The role of parameter uncertainties in the damage prediction of the alongwind-induced fatigue. Journal of Wind Engineering and Industrial Aerodynamics 104-106, 227-238.
Pagnini, L., Piccardo, G., 2017. A generalized gust factor technique for evaluating the wind–induced response of aeroelastic structures sensitive to vortex-induced vibrations. Journal of Fluids and Structures 70, 181-200.
Pagnini, L, Piccardo, G., 2021. Modal properties of a vertical axis wind turbine in operating and parked conditions. Engineering Structures 242, 112587.
Pagnini, L., Piccardo, G., Solari., G., 2020. VIV regimes and simplified solutions by the spectral model description. Journal of Wind Engineering and Industrial Aerodynamics 198, 104100.
Pagnini, L., Solari, G., 2001. Damping measurements of steel poles and tubular towers. Engineering Structures 23 (9), 1085-1095.
Repetto, M.P. and Solari, G., 2002. Dynamic crosswind fatigue of slender vertical structures. Wind and Structures 5, 527-542.
Repetto, M.P. and Solari, G., 2010. Wind-induced fatigue collapse of real slender structures. Engineering Structures 32, 3888–98.
Ruscheweyh, H., 1994. Vortex excited vibrations. In: Sockel H, editor. Wind-excited vibrations of structures. Wien, New York Springer Verlag. 51-84.
Vickery, B.J., Basu, R.I., 1983. Across-wind vibrations of structures of circular cross-section. Part I: development of a mathematical model for two-dimensional conditions. Journal of Wind Engineering and Industrial Aerodynamics 12 (1), 49–74.